Label-free biosensing using a photonic crystal structure in a total-internal-reflection geometry

Yunbo Guo*[a,b], Jing Yong Ye[a,b], Charles Divin[a], Thommey P. Thomas[b], Andrzej Myc[b], Tommaso F. Bersano-Begey[c], James R. Baker, Jr.[b], and Theodore B. Norris[a,b]

[a]Center for Ultrafast Optical Science, University of Michigan, Ann Arbor, MI 48109-2099, USA
[b]Michigan Nanotechnology Institute for Medicine and the Biological Sciences, University of Michigan, Ann Arbor, MI 48109-0648, USA
[c]Department of Biomedical Engineering, University of Michigan, Ann Arbor, MI 48109-2099, USA

ABSTRACT

A novel optical biosensor using a one-dimensional photonic crystal structure in a total-internal-reflection geometry (PC-TIR) is presented and investigated for label-free biosensing applications. This simple configuration forms a micro Fabry-Perot resonator in the top layer which provides a narrow optical resonance to enable label-free, highly sensitive measurements for the presence of analytes on the sensing surface or the refractive index change of the surrounding medium in the enhanced evanescent field; and at the same time it employs an open sensing surface for real-time biomolecular binding detection. The high sensitivity of the sensor was experimentally demonstrated by bulk solvent refractive index changes, ultrathin molecular films adsorbed on the sensing surface, and real-time analytes binding, measuring both the spectral shift of the photonic crystal resonance and the change of the intensity ratio in a differential reflectance measurement. Detection limits of 7×10^{-8} RIU for bulk solvent refractive index, 6×10^{-5} nm for molecular layer thickness and 24 fg/mm^2 for mass density were obtained, which represent a significant improvement relative to state-of-the-art surface-plasmon-resonance (SPR)-based systems. The PC-TIR sensor is thus seen to be a promising technology platform for high sensitivity and accurate biomolecular detection.

Keywords: Optical biosensors, photonic crystals, total internal reflection, Fabry-Perot resonator, evanescent field enhancement, label-free detection, real-time binding, refractive index

1. INTRODUCTION

With the advantages of robustness, simplicity and high sensitivity, optical biosensors have attracted significant attention for biomedical research, pharmaceutical discovery, environmental monitoring and homeland security [1]. Fluorescence-based optical detection is extremely sensitive, with a detection limit down to a single molecule [2], but requires labeling of target molecules. In contrast, label-free based detection measures analytes in their natural form, which avoids labeling processes and also allows for accurate, quantitative and kinetic measurement of molecular interactions. Sensing platforms based on surface plasmon resonance (SPR), interferometry, optical waveguides, optical ring resonators and photonic crystals, as well as many others, have been investigated [3]. The most widely used is the SPR-based biosensor [4-6], which detects the binding of analytes to ligands immobilized on a metal surface by measuring the effect of the bound molecules on the index of refraction seen by the SPR mode. Although SPR has become the dominant optical tool for biomolecular interaction studies, the sensitivity of SPR-based detection is not sufficient for applications that require detection of small molecules or low surface coverage (smaller than 1 pg/mm^2) of bound molecules [5, 6].

The key to obtaining higher sensitivity is clearly to employ an optical resonance which is narrower than the (very broad) surface plasmon resonance. Recently, photonic crystals (PCs) have been under intensive investigation as a novel label-free optical biosensing platform [7-12]. By introducing "defects" into the PCs structure, the electric field can be strongly confined and enhanced in the vicinity of the sensing surface where target analytes are adsorbed. Thus the corresponding optical spectrum shows narrow transmission peaks or reflection dips in the photonic bandgap, which enables highly sensitive biomolecular detection. Specifically, one-dimensional (1D) and two-dimensional (2D) photonic crystal structures fabricated from porous silicon have been developed [8, 9]; because the position of the cavity resonance is critically dependent on the index of refraction of the structures, adsorption of analyte molecules onto the porous silicon

* Email: guoybyw@umich.edu; Phone: (734)763-0209; Fax: (734)763-4876

Nanoscale Imaging, Sensing, and Actuation for Biomedical Applications VI
edited by Alexander N. Cartwright, Dan V. Nicolau, Proc. of SPIE Vol. 7188, 71880B
 · doi: 10.1117/12.808369

surfaces results in a measurable shift in the resonance. Although the porous-silicon biosensors provide higher sensitivity than SPR-based sensors, it is challenging to measure real-time binding kinetics due to the slow diffusion of biomolecules into the sub-micron pores.

In order to enable real-time binding measurements, one requires an open surface, which can be accessed optically via evanescent wave. In this paper, we present a novel optical sensor using a 1D PC structure in a total internal reflection (TIR) geometry (PC-TIR sensor). As discussed below, this PC-TIR sensor functions as a Fabry-Perot resonator, yielding a sharper resonance than the SPR sensor and hence a higher detection sensitivity, and yet the surface available for analyte binding is open to free space and allows real-time binding measurements. Similar structures, such as surface electromagnetic wave (SEW) excited in a Kretschmann-like geometry, have also been investigated [13-16]. However, the principle behind the appearance of the resonance in our structure has some important differences from SEW devices. Instead of an incomplete layer without absorption on top of a 1-D PCs in the SEW sensor, the resonance mode of our PC-TIR sensor is due to an intentionally inserted absorbing layer in the defect region of the PC structure. There is no surface-propagating wave present. The resonant PC structure defines a wavelength range over which the field is enhanced in the defect region, thus leading to selective absorption and the appearance of a resonance. This approach has a significant advantage in that the absorption can be engineered to yield an optimum resonance – i.e. an extra and highly controllable degree of freedom is available in the design. Besides this, our configuration possesses advantages of evanescent-field-based optical resonators without light- coupling problems, as the cavity Q is not made too large [17]. Moreover, the properties of PC structures make it easy to be designed and engineered to operate at any desired optical wavelength, and to detect analytes over a large dynamic range.

In the following, we first present the principle of the PC-TIR sensor, theoretically analyze its detection sensitivity, and then discuss how to make a suitable PC-TIR structure. Furthermore, we experimentally demonstrate its high sensitivity with bulk solvent refractive index changing, thin molecular films adsorption, and real-time protein binding.

2. PRINCIPLE

2.1 Sensing principle

Figure 1 (a) shows the schematic structure of the PC-TIR sensor. A one-dimensional photonic crystal (that is, an alternating pairs of dielectric layers) is grown on a substrate and a top layer is introduced on the PC structure as a "defect" layer. The light is incident through a coupling prism on the sensor with an angle chosen for total internal reflection at the last boundary between the higher-index defect layer and the lower-index surrounding medium. Therefore, a micro Fabry-Perot resonator is formed in the single defect layer by a high-reflecting PC structure and a TIR boundary. For light that is resonant with the cavity mode, the optical field will be enhanced near the surface of the defect layer, as Figure 1 (b) shows; light outside the photonic bandgap is reflected from the PC layers and has reduced field amplitude at the surface.

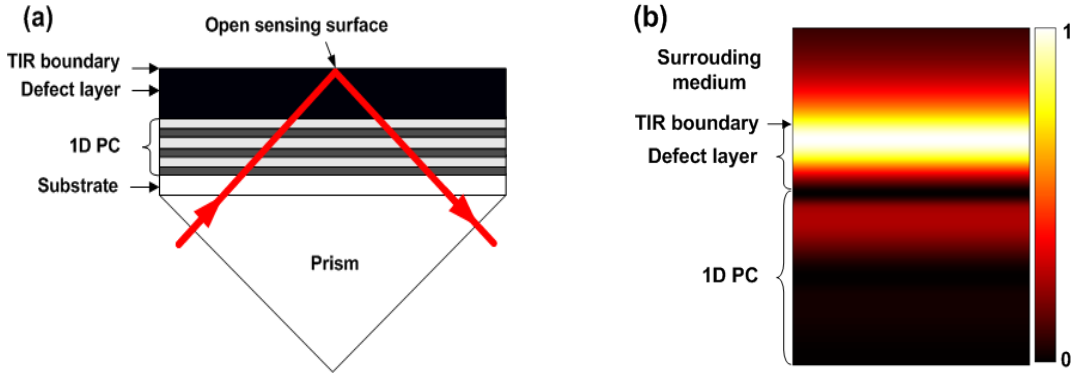

Fig.1 (a) Schematic of PC-TIR structure on a prism surface; (b) Electric field intensity distribution inside the PC-TIR structure and the evanescent field region.

Of course, light of all frequencies would be reflected from such a structure. In order to characterize the resonant mode of the Fabry-Perot microcavity, an energy loss mechanism is required. Here we incorporate a small amount of absorption in the defect layer; only light resonant with the microcavity mode is absorbed in this layer. Thus the reflectance spectrum of the total PC-TIR structure will show a pronounced dip at the resonant frequency, whose smallest reflectance can be engineered to be nearly zero by optimizing the absorption in the defect layer as shown in Figure 2. As

with SPR-based sensors, the analytes bound to the sensing surface do not need to absorb the light and the PC-TIR sensor is label-free.

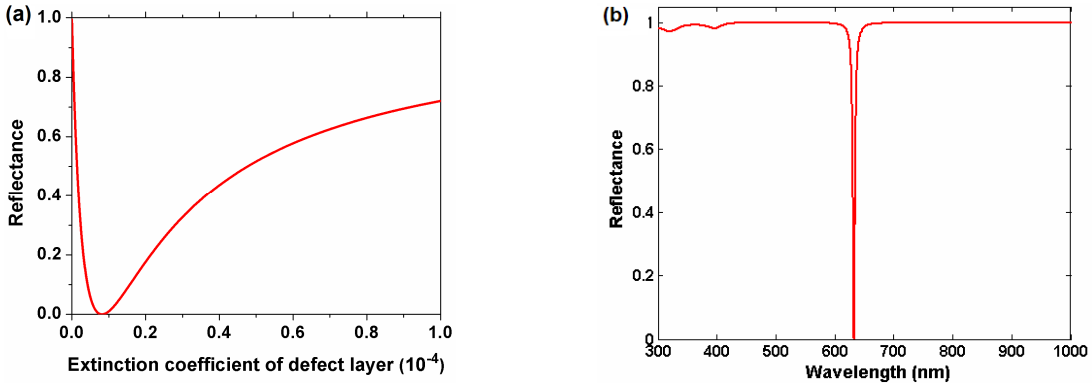

Fig. 2 (a) The relationship between the minimum reflectance and extinction coefficient of the defect layer; (b) A typical PC-TIR optical spectrum that shows a primary resonance dip at the resonant wavelength.

The operating principle of a PC-TIR sensor is as follows. Assume the incident angle at the substrate layer is θ_s, and the refraction angles in the lower index layer A, higher index layer B, and the defect layer X are θ_a, θ_b, and θ_x, respectively. Let n_s, n_a, n_b, and n_x be the refractive index of the substrate, lower index layer, higher index layer, and the defect layer, respectively. According to Snell's law,

$$n_s \sin\theta_s = n_a \sin\theta_a = n_b \sin\theta_b = n_x \sin\theta_x \qquad (1)$$

In order to form the photonic crystal structure, the thicknesses of dielectric multilayers should satisfy

$$n_a d_a \cos\theta_a = n_b d_b \cos\theta_b = \lambda_R / 4 \qquad (2)$$

where λ_R is the resonant wavelength, d_a, d_b represent physical thickness of the low and high index layers, respectively.

The thickness of the defect layer, d_x, is determined by the following resonant condition,

$$2 \cdot \frac{2\pi}{\lambda_R} n_x d_x \cos\theta_x + \alpha = (2m+1)\pi \qquad (m = 0,1,2,\ldots) \qquad (3)$$

where α represents the Goos-Hänchen phase shift between the defect layer and the surrounding medium. The factor of 2 in the first term on the left hand side is due to the fact that the light double passes the defect layer owing to the TIR.

One point worth noting is that the PC-TIR structure can be operated for both *S*- and *P*- polarized (also referred as transverse electric (TE) and transverse magnetic (TM)) light, which represents an advantage over SPR-based sensor that only works for *P*-polarized light [18, 19]. In the following study, we will emphasize *S*- polarized light.

For *S*-polarization of the incident light, the Goos-Hänchen phase shift is given by the following expression:

$$\alpha_s = -2\tan^{-1}\left(\left(\frac{n_S^2 \sin^2\theta_S - n_t^2}{n_x^2 - n_S^2 \sin^2\theta_S}\right)^{1/2}\right) \qquad (4)$$

where n_t is the refractive index of the surrounding medium on the defect layer.

If analyte molecules bind to ligands on the surface of the defect layer, they will give rise to a shift in the cavity resonance due to the phase shift seen by light propagating in the defect layer and undergoing TIR. Because of the field enhancement near the surface and the high Q of the microcavity, the shift can be very sensitive to molecular binding. Actually here two cases are possible. One is that the refractive index of molecule layer (adlayer) is so small that TIR happens between the defect layer and the adlayer, and the adlayer will change the effective refractive index of the surrounding medium in the evanescent region, just as in SPR-based sensors [20]; the other is that the refractive index of adlayer is large enough that TIR occurs between the adlayer and the surrounding medium. The latter case is not limited by the length of the evanescent region (~200nm); the resonant mode shifts within a wide bandgap (>500nm), and thus has a larger detection range than in the first case, or with SPR. Since normally the refractive index of molecules is large (~ 1.50) which is close to that of silica commonly made of dielectric layers of the PC structures, we will focus this study on the latter case.

The adlayer binding to the sensing surface will change the resonant condition to:

$$2 \cdot \frac{2\pi}{\lambda_R'}(n_x d_x \cos\theta_x + n_{ad} d_{ad} \cos\theta_{ad}) + \alpha' = (2m+1)\pi \qquad (m = 0,1,2,...) \qquad (5)$$

where n_{ad}, d_{ad} and θ_{ad} are the refractive index, thickness and refracted angle of the adlayer, respectively. λ_R' represents the new resonance wavelength, and α' is the effective Goos-Hänchen phase shift after the adlayer binding [21].

Therefore, by monitoring the reflectance response, one can detect the properties of adsorbed molecules (e.g. physical thickness or refractive index). There are two methods to measure the shift of the resonance dip. The first is to measure the resonance wavelength shift using a white light source and a spectrometer. However, the detection sensitivity is limited, mainly by the spectrometer resolution [22]. Much higher sensitivity can be obtained by performing an intensity measurement with a narrow-band optical probe tuned to the edge of the resonance line [22-25]. When a single-wavelength probe light is tuned near the half-width of the resonance dip, the reflected beam intensity varies sensitively with the analyte binding on the sensing surface due to the shift of the resonance dip wavelength λ_R.

2.2 Detection sensitivity

The overall sensitivity S of the PC-TIR sensor using the intensity detection approach depends on two figures of merit: the conversion efficiency of the resonant wavelength shift to the change of the intensity I_r (optical sensitivity O_s) and the conversion efficiency of molecular binding to resonant wavelength shift (binding sensitivity B_s). The latter term B_s is a function of the thickness (d_{ad}) and refractive index (n_{ad}) of the adlayer bound to the sensing surface; here we emphasize its relation with the adlayer thickness d_{ad}, and presume that the adlayer has essentially the same refractive index as the sensing surface:

$$S = \frac{\partial I_r}{\partial d_{ad}} = \frac{\partial I_r}{\partial \lambda_R} \cdot \frac{\partial \lambda_R}{\partial d_{ad}} = O_s \cdot B_s \qquad (6)$$

which indicates that the overall sensitivity S of the PC-TIR sensor is given by the product of O_s and B_s.

Since the resonance of the PC-TIR sensor is a Fabry-Perot cavity mode, its reflectance spectrum near the resonance can be described by the Lorentz equation as

$$I_r = I_0 \left[1 - \frac{1 - R_{\min}}{1 + \left(\frac{\lambda_R - \lambda_0}{\Delta\lambda / 2} \right)^2} \right] \qquad (7)$$

where I_0 is the incident probe light intensity, R_{min} is the minimum reflectance of the resonant dip, λ_0 is the initial resonance wavelength and $\Delta\lambda$ is the full width at half maximum (FWHM) of the resonance dip.

When $\lambda_R = \lambda_0 \pm 0.29\Delta\lambda$, the maximum optical sensitivity $O_{s,max}$ can be obtained

$$O_{s,\max} = \left(\frac{\partial I_r}{\partial \lambda_R} \right)_{\max} = \pm \frac{1.3 I_0 (1 - R_{\min})}{\Delta\lambda} \qquad (8)$$

The positive (negative) sign corresponds to the probe light wavelength lying on the lower (upper) side of resonant dip.

According to Equation (5), with the assumption $n_{ad} = n_x$, there is $\alpha' = \alpha$, and the binding sensitivity B_s can be expressed as

$$B_s = \frac{4\pi n_{ad} \cos\theta_{ad}}{(2m+1)\pi - \alpha} \qquad (9)$$

Substituting Equations (8) and (9) into Equation (6), one obtains the maximum overall sensitivity,

$$S_{\max} = \pm \frac{5.2\pi n_{ad} \cos\theta_{ad}}{[(2m+1)\pi - \alpha]} \frac{I_0 (1 - R_{\min})}{\Delta\lambda} \qquad (10)$$

Since the minimum reflectance R_{min} can be nearly 0 by optimizing the absorption in the defect layer, and smaller resonance dip width $\Delta\lambda$ can be easily obtained by increasing the number of the dielectric layers in the PC structures, the intensity detection mode may be used rather than the full spectral measurement in order to take the advantage of the narrow resonance dip of a PC-TIR microcavity, and thus achieve the highest possible sensitivity. Of course, Equation (10) also implies that intensity fluctuations of the incident probe light directly affect the PC-TIR sensor response. Thus a normalized reflectance method is required to suppress the effect of laser fluctuations [26]. As illustrated in Figure 5, a

Helium Neon (HeNe) probe laser beam was split into two and the ratio of the light intensity reflected from a binding area to a reference area of the sensor was measured.

3. MAKING A GOOD PC-TIR STRUCTURE

The detection sensitivity of the PC-TIR sensor is mainly decided by the resonant dip width, minimum reflectance and binding sensitivity, which further depends on the parameters of the PC-TIR structure: the refractive indices and thicknesses of the two dielectric constituents; the number of alternating multilayer; the operated angle; and the refractive index, thickness and absorption of the defect layer. We have selected carefully these parameters, with consideration to experimental conditions, to make a suitable structure.

First, titania (TiO_2) and silica (SiO_2) are chosen to be high and low refractive index materials, respectively. They are high-index-contrast and easily amenable to accurate fabrication by electron-beam (EB) evaporation. Their physical thicknesses are mainly decided by Equation (2). However, they may need to be tuned away a little from the ideal values to reduce the strong confinement of the PC structure, so that it is more flexible to manage suitable absorption in the defect layer.

Second, increasing the number of dielectric layers N can greatly narrow the resonant dip width $\Delta\lambda$, which is the pronounced advantage of our sensor. However, at the same time, it causes a stronger light confinement and the need for an optimal absorption to achieve minimum reflectance is reduced.

Third, the operating angle θ_i should be large enough that TIR occurs between the defect layer and the surrounding medium, but smaller than the critical angle for the dielectric layers. A small incident angle is preferred in the experiments, which is easier to achieve TIR and also produces less confinement.

Fourth, the defect layer X plays an extremely important role. On one hand, its refractive index affects the detect sensitivity (i.e. lower n_X brings larger B_S), and its thickness decides the position of resonant dip or the actual operated angle; on the other hand, its absorption affects the depth of resonant dip as Figure 2 (a) shows. However, when the structure exhibits very strong light confinement, the scattering loss between different media may dominate the achievable R_{min}. Therefore, there is a trade-off between resonant dip width $\Delta\lambda$ and minimum reflectance R_{min}. The structure should have a reasonable light confinement to obtain narrow $\Delta\lambda$, and also to keep the absorption in the defect layer much larger than the scattering loss (which is much more difficult to control). In previous fluorescence enhancement experiments [27], a dye-doped polymer film was spin-coated on the PC structure as the absorptive defect layer, but it is very hard to get a stable, uniform layer with accurate thickness and precise absorption, which is critical for further biomolecular detection. In our study, we choose pure silicon (Si) as a separate absorptive layer, as it is much easier to obtain a uniform and accurate thickness film on the top of the PC structure by EB evaporation. One more silica layer was deposited on top of the silicon layer as the final component of the defect layer. We note that the silica surface is commonly used in biomolecular studies and there are established methods for surface functionalization for molecular binding measurements.

According to the analysis above, we designed and fabricated a PC-TIR structure as shown in Figure 3 (a). The PC structure was composed of pairs of alternating 106-nm TiO_2 and 334-nm SiO_2 layers. An 18-nm Si thin layer was used as the absorptive layer and formed the defect layer with a 320-nm SiO_2 layer. The dielectric layers were coated by electron-beam deposition onto a BK-7 glass substrate with flatness of λ/10.

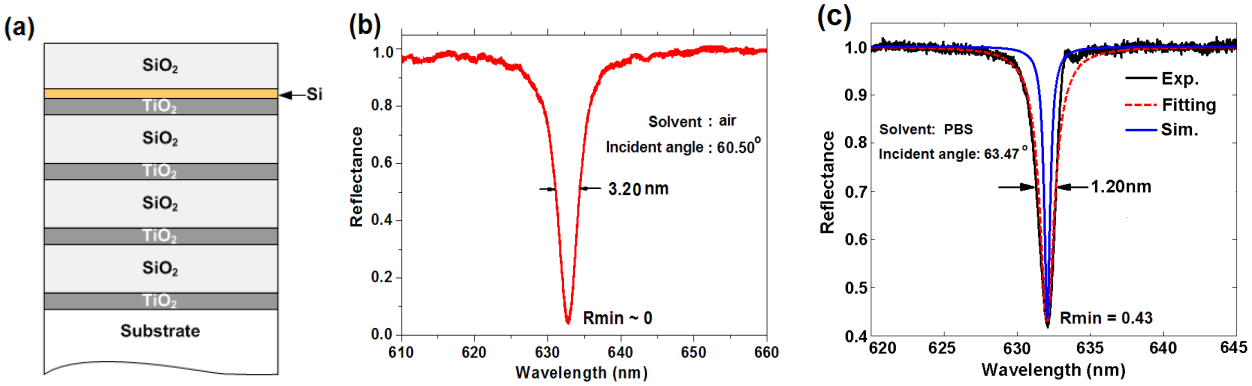

Fig.3 (a) PC-TIR sensor structure; (b) Reflectance spectrum when medium is air and incident angle is 60.50°; (c) Experimental, Lorentz fitting and simulated reflectance spectra when medium is PBS and incident angle is 63.47°.

Figure 3(b) shows the reflectance spectra of the PC-TIR sensor when the incident angle in the substrate θ_S was 60.50° and the surrounding medium was air (n_t = 1.0), showing a resonant dip with $\Delta\lambda$=3.20nm and R_{min} is near to 0. When the top sensing surface was covered by phosphate buffered saline (PBS, n_t = 1.3343) and the incident angle θ_S was tuned to 63.47°, we got a dip with resonant wavelength at 632.8nm, $\Delta\lambda$=1.20nm and R_{min} = 0.43, as Figure 3(c) shows. With larger θ_S and n_t (i.e., stronger light confinement), for the same structure, the resonant dip width $\Delta\lambda$ becomes narrower but R_{min} larger. In addition, Figure 3 (c) shows that the experimental reflectance spectrum is in reasonable agreement with a simulation using a transfer matrix calculation [28]. Although the resonance width is slightly larger than the simulated value of 0.60 nm due to non-uniformity of the deposited thin films, it is much narrower than that of a typical SPR resonance [6], and allows more sensitive detection of resonance shifts. Moreover, Figure 3(c) also shows that the reflectance spectrum near the resonance can be well-fit by a Lorentzian lineshape as the resonance of the PC-TIR sensor is a Fabry-Perot cavity mode. Of course, a better resonant dip (with narrower $\Delta\lambda$ and smaller R_{min}) can be achieved by further optimizing the parameters of the PC-TIR structure and improving the uniformity and quality of the deposited dielectric layers.

4. EXPERIMENTS

4.1 Experiment setup

Figure 4 shows our experimental setup. It combines the white light spectral measurement and the laser intensity measurement in one system. For spectral measurements, the reflectance was measured using a white light source. The beam was coupled with an objective lens into a single-mode optical fiber to obtain a good spatial beam profile and was collimated with a second objective lens. A linear polarizer was used to select *S* - polarized light, and a 1-mm pinhole (PH2) was used to set the size of the probe beam. The beam was incident on the PC-TIR sensor with an incident angle controlled using a high precision programmed rotation stage. The reflected beam was propagated into a spectrometer (Jobin Yvon iHR550) with a resolution of 0.025 nm to measure the reflectance spectrum around the resonance dip. For intensity measurements, a single-wavelength laser (HeNe laser) was used and the collimated laser beam traveled the same path as the white light except that the reflected light was directly detected using a pair of photodiode detectors. The ratio of the light intensity reflected from a binding area to a reference area of the sensor was measured. These two measurements could be easily switched by moving mirror M2, which enabled us to monitor the molecular binding with spectral shift and intensity ratio change almost concurrently. The PC-TIR sensor was put on the prism via immersion oil and was stabilized, and the top surface was attached to a microfludics cell with two parallel flow channels; the solutions were introduced by a withdrawing pump, and the flow rate could be adjusted over a large range (0 to 10.00mL/min).

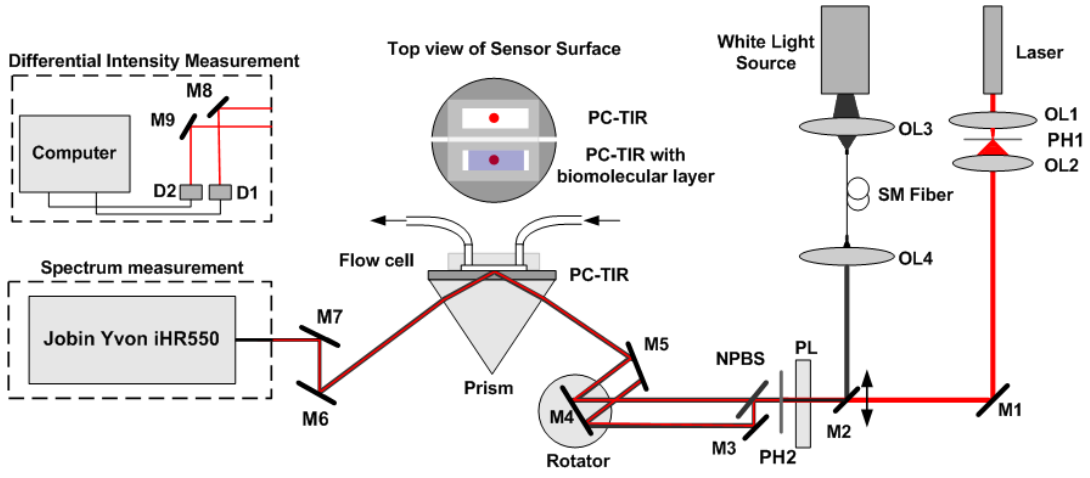

Fig. 4. Experimental setup for spectral and differential reflectance measurements. OL1-OL5: objective lenses, SM fiber: single mode fiber, PH1-PH2: pinhole, PL: polarizer, NPBS: Non-polarizing beam splitter, M1-M9: reflecting mirrors, D1-D2: photodiode detectors.

Similar to SPR-based systems, our present experimental setup is characterized by a short term noise floor and a long term drift limited by the mechanical stability of the system, respectively. As Figure 5 shows, the fluctuation of the signal channel was 2.2×10^{-3} (5.6×10^{-4} over 0.25829) about 100 times higher than that of the intensity ratio 2.2×10^{-5} (1.8×10^{-5}

over 0.81674). It means that differential reflectance measurement can greatly suppress the noise floor. Over a typical molecular binding period (120 seconds), with a 1-Hz signal bandwidth, both the differential reflectance noise floor (i.e., standard deviation) and long term drift are below 2.2×10^{-5}. Furthermore, the noise of the presented system could be further decreased by improving the quality and uniformity of the PC-TIR structure, by controlling temperature stabilization and by decreasing the laser fluctuation.

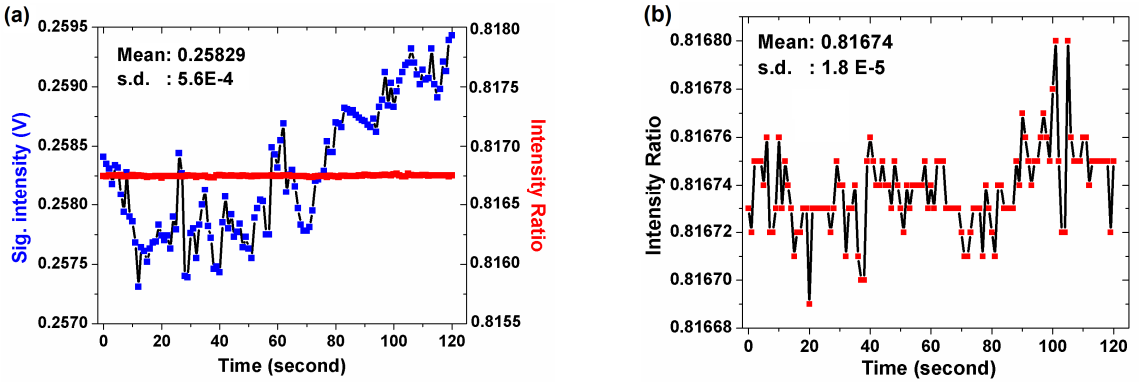

Fig. 5 (a) Fluctuations of the signal channel intensity and of intensity ratio; (b) Fluctuation of intensity ratio low to 2.2×10^{-5}.

4.2 Angular sensitivity

When the incident angle changes, the resonant wavelength shifts in order to satisfy the resonant condition described in Equation (3). Figure 6 shows that the experimental data has a good agreement with the simulated results, and the angular sensitivity of the PC-TIR sensor is - 43.9nm per degree. By adjusting the incident angle, it is easy to tune the resonant wavelength so that the probe laser lies within the resonant dip for intensity measurements.

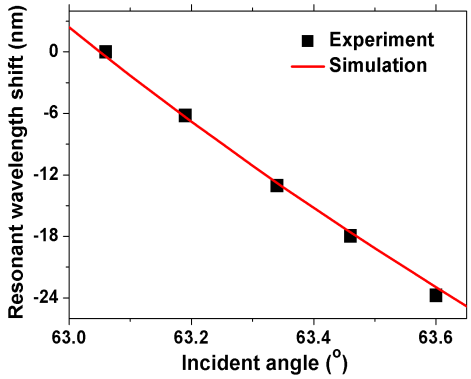

Fig. 6 The resonant wavelength shifts with incident angle changing

4.3 Bulk solvent refractive index sensitivity

Similarly, from resonant condition Equations (3) and (4), we can derive the relationship between the shift of resonant wavelength and the change of bulk solvent refractive index, and the sensitivity S_{sol} is expressed as

$$S_{sol} = \frac{\partial \lambda_R}{\partial n_t} = \frac{\partial \lambda_R}{\partial \alpha_S} \bullet \frac{\partial \alpha_S}{\partial n_t} = \frac{\lambda_R{}^2 n_t}{2\pi d_x (n_x{}^2 - n_t{}^2)\sqrt{n_S^2 \sin^2 \theta_S - n_t^2}} \qquad (11)$$

This equation indicates that the resonant wavelength shifts to longer wavelength and that the sensitivity becomes higher with larger n_t.

In our experiments, the bulk solvent refractive index sensitivity is characterized by a series of different concentrations of ethylene glycol solution in de-ionized (DI)-water, whose refractive indices are shown in Figure 7(a). And Figure 7(b) shows the resonant wavelength shift with different concentrations of ethylene glycol solution on the sensing surface. The experimental data is fitted well with the simulation results, and appears the same properties as

Equation (11). A sensitivity of 1490 nm/RIU was then obtained by measuring the slope of the resonant wavelength shift versus RI change.

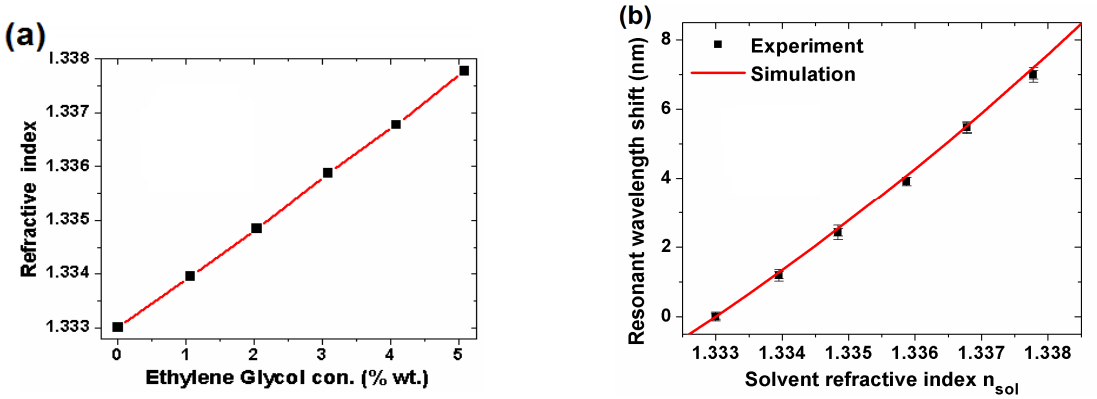

Fig.7 (a) Bulk solvent refractive index for different concentrations of ethylene glycol solution in DI-water (0%, 1%, 2%, 3%, 4%, 5%); (b) Resonance wavelength shifts with different refractive indices solution on the sensing surface.

As we mentioned before, there are two detection methods. The spectrum measurement is limited by the available spectrometer resolution. For example, here the spectrometer resolution is 0.025 nm, so the detection limit for bulk solvent refractive index of our PC-TIR sensor is 1.7×10^{-5} RIU. However, the differential reflectance measurement can achieve a much higher sensitivity (thus a lower detection limit).

In order to demonstrate this, we adjusted the incident angle so that HeNe wavelength (632.8nm) was at the long-wavelength half-maximum point in the resonant dip, and then 0 to 1% ethylene glycol solutions were flowed over the sensing surface consecutively with a rinsing step (by DI-water) between each new concentration to ensure the surface was cleaned before the next measurement. The real-time differential reflectance ratio was measured and a much large signal change was obtained and shown in Figure 8 (a). For example, the refractive index of 0.5% ethylene glycol solution is 5×10^{-4} RIU larger than that of DI-water, but the ratio change is 0.16439. Taking the noise floor 2.2×10^{-5} for the differential reflectance ratio as the smallest detectable signal, the detection limit (*DL*) for bulk solvent refractive index is

$$DL_{sol} = \frac{\delta R}{\Delta R} \bullet \Delta n = \frac{2.2\times10^{-5}}{0.16439} \bullet 5\times10^{-4}\, RIU \approx 6.7\times10^{-8}\, RIU \qquad (12)$$

that is about 250 times lower than that of spectrometer measurement.

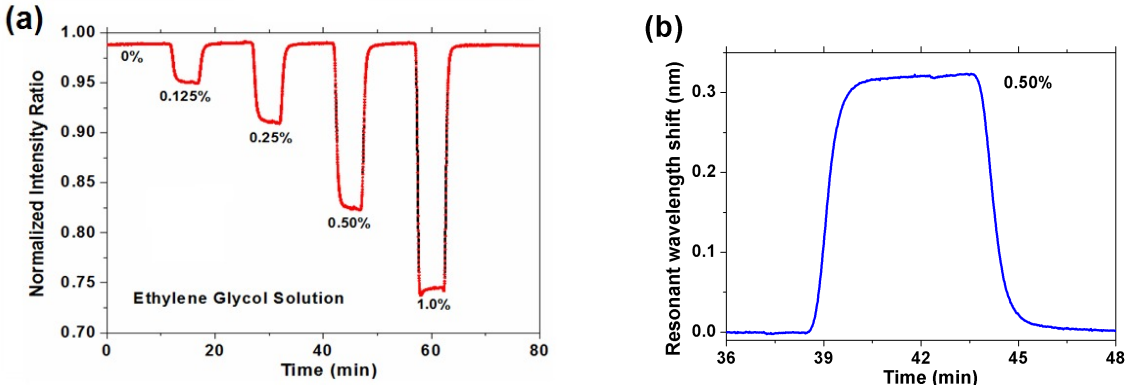

Fig.8 (a) Normalized differential ratio with different conc. of ethylene glycol solution; (b) Transformed resonant wavelength shift with flowing 0.50% ethylene glycol solution.

Actually there are two ways to measure resonant wavelength shift with bulk solvent refractive index changing or molecular binding. One is to make use of the linear region of the resonant dip [24, 25], as Equation (12) shows; the other is to transform the differential intensity ratio change to the resonant wavelength shift directly by the reversed Lorentz formula (Equation (13)), as the resonant dip can be well fitted by a Lorentzian lineshape (as shown in Figure 3 (c)). The latter one makes it easier to determine the bulk solvent refractive index change or molecular binding in real time.

$$\Delta\lambda_{Res.} = \lambda_{Res.} - \lambda_0 = \left(\lambda_{Laser} \mp \frac{\Delta\lambda}{2} \sqrt{\frac{R - R_{\min}}{1 - R}} \right) - \lambda_0 \qquad (\lambda_{Res.} < \lambda_{Laser} \ \ or > \lambda_{Laser}) \tag{13}$$

Figure 8 (b) shows the data transformed into resonant wavelength shift, and the final shift is 0.32271 nm for the bulk solvent refractive index change of 5×10^{-4} RIU. Moreover, the noise floor 2.2×10^{-5} for differential reflectance ratio is corresponding to 4.4×10^{-5} nm for resonant wavelength shift, so the detection limit for bulk solvent refractive index can be calculated to be

$$DL_{sol} = \frac{\delta\lambda}{\Delta\lambda} \bullet \Delta n = \frac{4.4\times10^{-5}}{0.32271} \bullet 5\times10^{-4} RIU \approx 6.8\times10^{-8} RIU \tag{14}$$

which is almost the same as obtained by Equation (13).

4.4 Thin molecular layer detection

In order to characterize the high sensitivity of PC-TIR sensor for biomolecular assay, we used two coupling agents, aminopropyltriethoxysilane (APTES) and glutaraldehyde, which can form uniform thin layers on silica surfaces [29]. The sensing surface was first cleaned by a piranha solution (H_2SO_4 (95%) / H_2O_2 (30%) = 3:1), and then exposed to 5% APTES in H_2O and methanol (1:1) solution for 20 minutes, then rinsed with DI water and dried with air. After the silanization, a thin layer of APTES molecules was formed on the sensing surface. Then the sensor was exposed to a 2.5% glutaraldehyde solution in 20 mM HEPES buffer (pH=7.4) for 30 minutes and rinsed with DI water and dried with air. A thin layer of glutaraldehyde molecules was adsorbed on the surface due to the reaction with the amino groups on the silanized surface.

By spectroscopic ellipsometry measurements, we found the APTES monolayer and APTES/glutaraldehyde bilayer to be 0.55±0.04 nm and 1.31±0.04 nm respectively, assuming the refractive indices of APTES and glutaraldehyde to be 1.46. The shift of the PC-TIR resonance as the layers were adsorbed was first observed by measuring the reflectance spectrum. The results, shown in Figure 9 (a), revealed a resonant wavelength shift of 0.52 and 1.18 nm respectively, as the APTES monolayer and APTES/glutaraldehyde bilayer were formed. Their physical thicknesses adsorbed on the sensing surface are calculated to be 0.62 and 1.39 nm from the transfer matrix simulation, which are in approximate agreement with the ellipsometry measurement.

In addition, the differential reflectance ratio change was observed. Taken as a reference point, the ratio for the bare PC-TIR sensor changed from 1.00000 to 0.77814 for the binding of an APTES monolayer (data in Figure 9 (b)). Similarly, taking the noise floor 2.2×10^{-5} as the smallest detectable signal, the detection limit of our PC-TIR sensor for analyte layer thickness is thus estimated to be 0.55 nm × (2.2×10^{-5}/0.22186) ~ 6×10^{-5} nm. This thickness detection limit corresponds to 10^{-4} monolayers, which represents an order-of-magnitude improvement over conventional SPR based measurements [20, 25]. Moreover, the resonance width of the PC-TIR sensor can be made much narrower by increasing the number and uniformity of dielectric layers in the structure, in contrast to a fixed SPR bandwidth of a metal film.

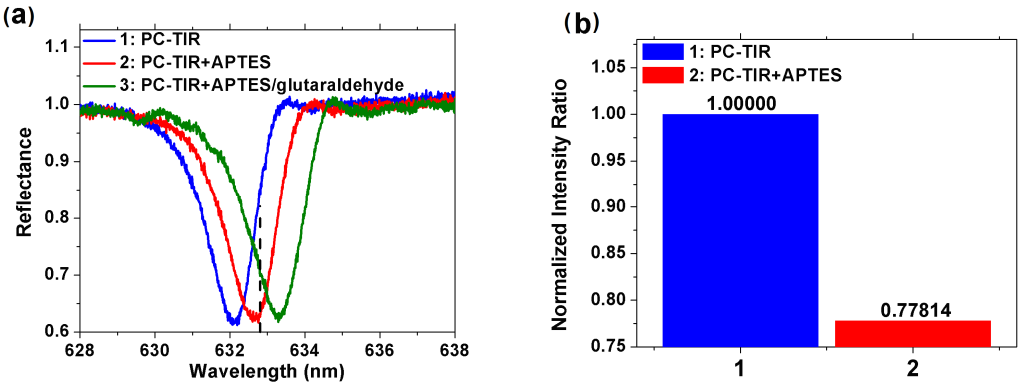

Fig.9 (a) Resonance dip wavelength shifts with the binding of adlayer; (b), Reflectance ratios at 632.8 nm from differential reflectance measurements for a PC-TIR sensor without treatments and with APTES monolayer.

4.5 Real-time protein binding

One of the advantages of our PC-TIR sensor is an open sensing surface, which can be used to combine with microfludics devices and to measure real-time analytes binding. Here the well-studied biotin-streptavidin system with its extremely high binding affinity (K_d ~10^{-15}M) is chosen to illustrate the attributes of the PC-TIR sensor [29, 30]. The biotin-streptavidin system has been studied in great detail and serves as an excellent model system for biomolecular recognition. Moreover, streptavidin is a tetrameric protein which can bind up to four biotinlyated molecules with minimal impact on its biological activity and therefore allows for extending the analyte accessibility of the sensor.

To create a biotin-functionalized sensor for capturing streptavidin (SA), the sensing surface (silica) was first cleaned and oxidized by the piranha solution (H_2SO_4 (95%) / H_2O_2 (30%)=3:1), then silanized with 5% APTES solution in methanol/ water (1:1). Next, Sulfo-NHS -LC-LC-Biotin (1 mg/mL in PBS) was flowed into the flow cell for several minutes and then the flow was stopped for several hours so that the NHS-activated biotin reacted efficiently with the primary amino groups to form stable amide bonds. After that, 0.5 mg/mL bovine serum albumin (BSA) in PBS was flowed to block the non-specific binding sites of the streptavidin protein with the silica sensing surface.

After surface functionalization, PBS buffer was kept flowing over the sensing surface for sufficient time to get a stable baseline. At time zero, 1 μg/mL streptavidin solution in PBS was injected into the flow cell with a flow rate 100 μL/min, and then washed by PBS. This procedure was monitored in real time. In Figure 10 (a), one can see that the resonant wavelength shifted by 0.54 nm with streptavidin binding to the biotinlyated surface. Assuming that the refractive index of streptavidin is 1.45, its effective physical thickness adsorbed on the sensing surface is 0.60 nm by a transfer matrix simulation, which is about 10% of that of streptavidin monolayer [30]. This corresponds to 10% of the typical streptavidin saturation coverage or an average packing density of 2.4×10^9 molecules/mm^2 [25, 31]. Since our PC-TIR sensor can resolve a resonant wavelength shift down to 4.4×10^{-5} nm, the 0.54-nm streptavidin layer in the experiment was detected with a signal to noise ratio of ~ 10^4. Therefore the minimal density that can be measured by our sensor is 2.4×10^5 molecules/mm^2, which corresponds to a mass density detection limit 24 fg/mm^2 for streptavidin (MW ~ 60,000), orders of magnitude lower than that of SPR-based sensors [5, 6].

As discussed above, a streptavidin molecule has four biotin-binding pockets. One or two may be attached to the biotin on the surface, the remaining two or three still available to bind biotin-conjugated analytes. Here we give an example, 10 μg/mL biotin-conjugated IgG in PBS was used as a target analyte and flowed over the biotin-streptavidin adsorbed surface. The sensorgram was shown as Figure 10 (b), and the adsorption of biotin-conjugated IgG on the sensing surface caused a resonant wavelength shift of 0.30 nm. The shift is reasonable, considering that several biotin molecules may be conjugated on one IgG antibody molecule.

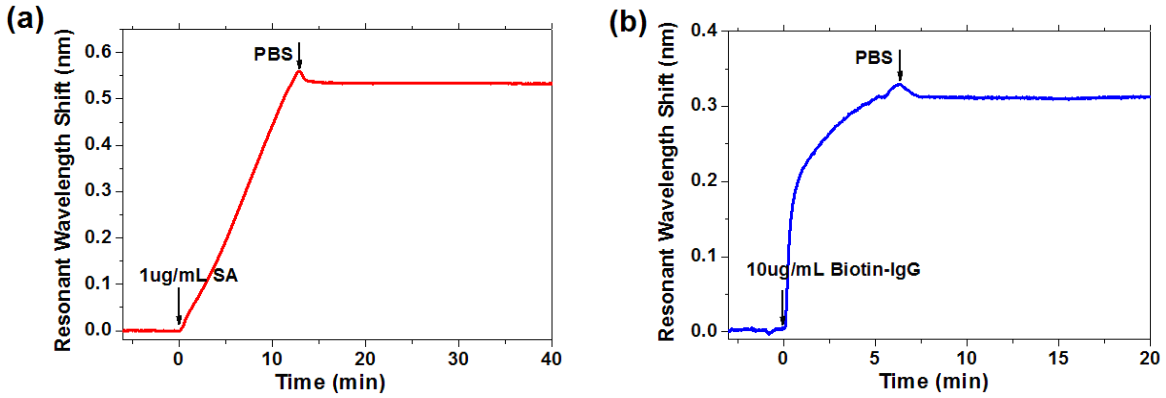

Fig.10 (a) Detection of SA binding to biotinlyated surface; (b) Biotin-conjugated IgG binding to SA-adsorbed surface.

5. CONCLUSIONS

To summarize, we have developed a novel optical biosensor based on a PC structure used in a TIR configuration, which provides an open interface allowing easy access for sensitive real-time analyte measurements. We have demonstrated the operation of the sensor and determined its detection limit by observing the change of bulk solvent refractive index, the adsorption of thin molecular films, and real-time protein binding. Ultra low detection limits were experimentally shown for the PC-TIR sensor in comparison with that of state-of-the-art SPR sensors [3-6, 20, 32].

Besides label-free detection, the high evanescent-field enhancement in the PC-TIR sensor may be exploited for sensitive fluorescence or Raman measurements, such as total internal reflection fluorescence (TIRF) [33], total internal reflection- fluorescence correlation spectroscopy (TIR-FCS) [34] or stimulated enhanced Raman scattering (SERS) [35]; these may be incorporated with real time binding measurements to provide comprehensive information on biomolecular interactions on the sensing surface [36, 37].

Furthermore, by integrating with the technologies of microfludics [38], optical fibers or waveguides, micro-array laser sources or detectors [39], surface functionalization/patterning, nano-fabrication and many others [3, 5], the PC-TIR sensor shows a great potential to be a high-sensitivity, high-throughput lab-on-a-chip sensing platform for biomolecular analysis and medical diagnoses.

ACKNOWLEDEGEMENTS

This project has been funded in whole or in part with Federal funds from the National Cancer Institute, National Institutes of Health, under award 1 R21 RR021893. Y. Guo gratefully acknowledges Riethmiller Fellowship of the University of Michigan for financial support.

REFERENCES

[1] Narayanaswamy, R. and Wolfbeis, Otto S., [Optical Sensors: Industrial, Environmental and Diagnostic Applications], Springer, New York (2004).

[2] Moerner, W. E., "New directions in single-molecule imaging and analysis," Proc. Natl. Acad. Sci. 104, 12596-12602 (2007).

[3] Fan, X., White, I. M., Shopova, S. I., Zhu, H., Suter, J. D. and Sun, Y., "Sensitive optical biosensors for unlabeled targets: A review," Anal. Chim. Acta. 620, 8-26 (2008).

[4] Homola, J., "Surface plasmon resonance sensors for detection of chemical and biological species," Chem. Rev. 108, 462-493 (2008).

[5] Hoaa, X. D., Kirk, A.G. and Tabrizian, M., "Towards integrated and sensitive surface plasmon resonance biosensors: A review of recent progress," Biosensors and Bioelectronics 23, 151-160 (2007).

[6] Homola, J.,"Present and future of surface plasmon resonance biosensors,"Anal. Bioanal. Chem.377, 528-539 (2003).

[7] Cunningham, B.T., Laing, L., "Microplate-based, label-free detection of biomolecular interactions: applications in proteomics," Expert Rev. Proteomics 3, 271-281 (2006).

[8] Ouyang, H., Striemer, C. C. and Fauchet, P. M., "Quantitative analysis of the sensitivity of porous silicon optical biosensors," Appl. Phys. Lett. 88, 163108 (2006).

[9] Lee, M. R. and Fauchet, P. M., "Two-dimensional silicon photonic crystal based biosensing platform for protein detection," Opt. Express 15, 4530-4535(2007).

[10] Kang, C. and Weiss, S. M., "Photonic crystal with multiple-hole defect for sensor applications," Opt. Express 16, 18188-18193 (2008).

[11] Rindorf, L. and Bang, O., "Highly sensitive refractometer with a photonic-crystal-fiber long-period grating," Opt. Lett. 33, 563-565 (2008).

[12] Mandal, S. and Erickson, D., "Nanoscale optofluidic sensor arrays," Opt. Express 16, 1623-1631 (2008).

[13] Robertson, W. M. and May, M. S., "Surface electromagnetic wave excitation on one-dimensional photonic band-gap arrays," Appl. Phys. Lett. 74, 1800-1802 (1999).

[14] Villa, F., Regalado, L. E., Ramos-Mendieta, F., Gaspar-Armenta, J. and Lopez-Rios, T., "Photonic crystal sensor based on surface waves for thin-film characterization," Opt. Lett. 27, 646-648 (2002).

[15] Konopsky, V. N. and Alieva, E. V., "Photonic crystal surface waves for optical biosensors," Anal. Chem. 79, 4729-4735 (2007).

[16] Usievich, B. A., Svetikov, V. V., Nurligareev, D. Kh. and Sychugov, V.A., "Surface waves at the boundary of a system of coupled waveguides," Quant. Electr., 37, 981-984 (2007).

[17] Lechuga, L. M., "Optical sensors based on evanescent field sensing - Part II. Integrated optical sensors," Quim. Anal. 19, Suppl. 1, 61-67 (2000).

[18] Nelson, R. L. and Haus, J. W., "One-dimensional photonic crystals in reflection geometry for optical applications," Appl. Phys. Lett. 83, 1089-1091 (2003).

[19] Zhan, Q., "Enhancement of fluorescence signal with one dimensional photonic band gap structure, " Proc. SPIE 6444, 644408 (2007).
[20] Jung, L. S., Campbell, C. T., Chinowsky, T. M., Mar, M. N. and Yee, S. S., "Quantitative interpretation of the response of surface plasmon resonance sensors to adsorbed films," Langmuir 14, 5636-5648 (1998).
[21] Kaiser, R., Levy, Y., Vansteenkiste, N., Aspect, A., Seifert, W., Leipold, D. and Mlynek, J., "Resonant enhancement of evanescent waves with a thin dielectric waveguide," Opt. Commun. 104, 234-240 (1994).
[22] Schmidt, O., Kiesel, P., Mohta, S. and Johnson, N. M., "Resolving pm wavelength shifts in optical sensing," Appl. Phys. B, 86, 593-600 (2007).
[23] Ran, B. and Lipson, S. G., "Comparison between sensitivities of phase and intensity detection in surface plasmon resonance," Opt. Express 14, 5641-5650 (2006).
[24] Liu, X., Cao, Z., Shen, Q. and Huang, S., "Optical Sensor Based on Fabry-Perot Resonance Modes," Appl. Opt. 42, 7137-7140 (2003).
[25] Shurnaker-Parry, J. S. and Campbell, C. T., "Quantitative methods for spatially resolved adsorption/desorption measurements in real time by surface plasmon resonance microscopy," Anal. Chem. 76, 907-917 (2004).
[26] Myszka, D. G., "Improving biosensor analysis," J. Mol. Recognit., 12, 279-284 (1999).
[27] Inouye, H., Arakawa, M., Ye, J. Y., Hattori, T., Nakatsuka, H. and Hirao, K., "Optical properties of a total-reflection- type one-dimensional photonic crystal," IEEE J. Quant. Electr. 38, 867-871(2002).
[28] Knittl, Z., [Optics of Thin films (An Optical Multilayer Theory)], Wiley, London (1976).
[29] Hermanson, G. T., [Biocojugate Techniques], Academic Press, New York (1996).
[30] Busse, S., Scheumann, V., Menges, B. and Mittler, S., "Sensitivity studies for specific binding reactions using the biotin/streptavidin system by evanescent optical methods," Biosens. Bioelectron. 17, 704-710 (2002).
[31] Jung, L. S., Nelson, K. E., Stayton, P. S. and Campbell, C. T., "Binding and dissociation kinetics of wild-type and mutant streptavidins on mixed biotin-containing alkylthiolate monolayers," Langmuir 16, 9421-9432 (2000).
[32] Stewart, C. E., Hooper, I. R. and Sambles, J. R., "Surface plasmon differential ellipsometry of aqueous solutions for bio-chemical," J. Phys. D: Appl. Phys. 41,105408 (2008).
[33] He, R., Chang, G., Wu, H., Lin, C., Chiu, K., Su, Y. and Chen, S., "Enhanced live cell membrane imaging using surface plasmon-enhanced total internal reflection fluorescence microscopy," Opt. Express 14, 9307-9316 (2006).
[34] Thompson, N. L. and Steele, B. L., "Total internal reflection with fluorescence correlation spectroscopy," Nat. Protoc. 2, 878-890 (2007).
[35] White, I. M., Gohring, J. and Fan, X., "SERS-based detection in an optofluidic ring resonator platform," Opt. Express 15, 17433-17442 (2007).
[36] Hu, W. P., Chen, S. J., Yih, J. N., Lin, G. Y. and Chang, G. L., "Studying protein structural changes based on surface plasmon resonance and surface-enhanced Raman scattering," Proc. SPIE 5327, 88-94 (2004).
[37] Loncar, M., "Molecular sensors: Cavities lead the way," Nat. Photonics 1, 565 - 567 (2007)
[38] Monat, C., Domachuk, P. and Eggleton, B. J., "Integrated optofluidics: A new river of light," Nat. Photonics 1, 106-114 (2007).
[39] Bally, M., Halter, M., Voros, J., Grandin, H. M., "Optical microarray biosensing techniques," Surf. Interface Anal. 38, 1442–1458 (2006).